Reprinted from The Journal of Physical Chemistry, 1995, 99.

Electronic Transition Oscillator Strength by the Extended Hückel Molecular Orbital Method

Gion Calzaferri* and Ruedi Rytz

Institute for Inorganic and Physical Chemistry, University of Berne, Freiestrasse 3, CH-3000 Bern 9, Switzerland

Received: January 12, 1995[⊗]

Calculations of the oscillator strength of electronic dipole-induced transitions (EDiTs) based on EHMO wave functions including all transition matrix elements offer a generally applicable method for computing intensities of all types of transitions found in molecules, clusters, and complexes. Application of this EHMO−EDiT procedure to formaldehyde, MnO_4^-, *p*-(*N*,*N*-dimethylamino)benzonitrile (DMABN), 2,2′-bipyridyl (bpy), Ru(bpy)$_3^{2+}$, and [Co(CO)$_4$($H_7Si_8O_{12}$)] illustrates the versatility of this procedure and offers new insight into some "old problems". We find that the TICT state of DMABN is expected to live long enough to relax to a state described by the $(b_1)^1(b_2)^1$ configuration. Emission of a photon in this state is forbidden by symmetry. However, a small twist of the dialkylamino group by only 15° increases this oscillator strength along the *z* axis enormously. TICT emission has empirically been shown to be *z*-polarized and strong in intensity. The emission rates can be thermally activated. This is in good qualitative agreement with the oscillator strength calculation. We also find that the intensities of the two *z*-polarized $\pi^* \leftarrow \pi$ transitions depend relatively little on the amino group torsional angle. This dependence is indeed characteristic for the TICT state. EDiT calculations on bpy as a function of the torsional angle θ lead to a satisfactory interpretation of the two prominent $\pi^* \leftarrow \pi$ transitions of this very often used ligand. The $2\pi^* \leftarrow$ 2n oscillator strength is very small for cis. However, the cis $(2n)^1(2\pi^*)^1$ configuration correlates with the trans $(1\pi)^1(1\pi^*)^1$ which bears a large $1\pi^* \leftarrow 1\pi$ oscillator strength. The cis $2\pi^* \leftarrow 1\pi$ transition retains its $\pi^* \leftarrow \pi$ character but loses intensity with increasing θ and becomes symmetry-forbidden at $\theta = 180°$. The first intense band which is broad, featureless, and very similar in different organic solvents is the result of a superposition of bands arising from an equilibrium Boltzmann distribution over the whole range of angles θ from 0° to 180°. This causes a hypsochromic shift of the maximum of the first intense band, because the $1\pi^* \leftarrow 1\pi$ transition energies of the species with angles different from $\theta \approx 180°$ and $\theta \approx 0°$ appear at larger energy. The bathochromic shift of the first $1\pi^* \leftarrow 1\pi$ transition of the protonated bpy is due to the predominance of the cis isomer and hence a narrow Boltzmann distribution of the θ region close to 0°. The number of possible Ru(bpy)$_3^{2+}$ excited-state configurations in the HOMO/LUMO region give rise to 143 different one-electron spin-allowed transitions. Even though a few of them are forbidden by symmetry, most are allowed, but many are of low intensity. They can be grouped according to the usual classification MLCT($\pi^* \leftarrow$ d), MC(d* ← d), LC($\pi^* \leftarrow \pi$,$\pi^* \leftarrow$ n), and LMCT(d* ← π,d* ← n), which is based on the orbitals engaged and on the specific parts of the complex involved. However, the absorption around 40 000 cm^{-1} is composed of a LC($\pi^* \leftarrow \pi$)-type and a LMCT(d−n* ← 1π)-type transition. Thus, the often encountered opinion that this region has to be attributed to a MLCT transition should be revised. The HOMO of [Co(CO)$_4$($H_7Si_8O_{12}$)] consists of oxygen lone pairs localized on $H_7Si_8O_{12}$, and the LUMO is identical with the LUMO of Co(CO)$_4$. The first electronic transitions observed in the near-UV are of the $H_7Si_8O_{12}$ (oxygen lone pair) to Co(CO)$_4$ fragment charge-transfer type.

I. Introduction

Electronic transitions are usually classified according to the orbitals engaged or to specific parts of the molecule involved. Common types of electronic transitions in organic compounds are $\pi^* \leftarrow \pi$, $\sigma^* \leftarrow \sigma$, $\pi^* \leftarrow$ n, and π^*(acceptor) ← π(donor), the latter leading to so-called locally excited (LE) states. Metal-centered (MC), ligand-centered (LC), ligand-to-metal charge-transfer (LMCT), and metal-to-ligand charge-transfer (MLCT) transitions are commonly observed in coordination compounds. The basic theoretical conception for calculating intensities of electronic dipole-induced transitions is the same in all these cases and was outlined by R. S. Mulliken more than 50 years ago.[1] Calculations of oscillator strengths for $\pi^* \leftarrow \pi$ transitions based on the PPP[2] method have long been a useful tool for spectroscopic and photochemical studies. Wolfsberg and Helmholz were the first to explain why the tetrahedral ions MnO_4^- and CrO_4^{2-} are colored while the isoelectronic ClO_4^-, SO_4^{2-}, and PO_4^{3-} are not, based on LCAO−MO calculations of the extended Hückel type and on computed oscillator strengths.[3a] Oscillator strength calculations on different levels of sophistication are often used. However, a general procedure which can be applied to compute or estimate intensities of all types of electronic dipole-induced transitions (EDiTs) of large molecules and complexes has still been missing. The simplest generally applicable method bearing the potential to fill this gap is the extended Hückel molecular orbital (EHMO) theory.[4] One of the most fascinating aspects of this transparent method is that it can be successfully applied to study molecules, clusters, complexes, solids, and the interaction of molecules on surfaces.[5−7] We have therefore developed an EDiT program to calculate oscillator strengths of even very large molecules and complexes based on Slater-type MOs. Calculations of the two-center

* Author to whom correspondence should be addressed.
⊗ Abstract published in *Advance ACS Abstracts,* July 15, 1995.

0022-3654/95/2099-12141$09.00/0

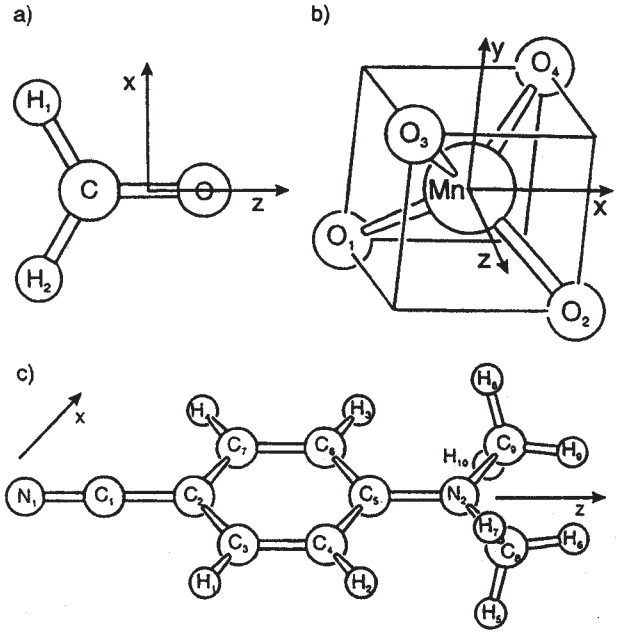

Figure 1. (a) Formaldehyde, (b) permanganate ion, and (c) *p*-(*N*,*N*-dimethylamino)benzonitrile (DMABN).

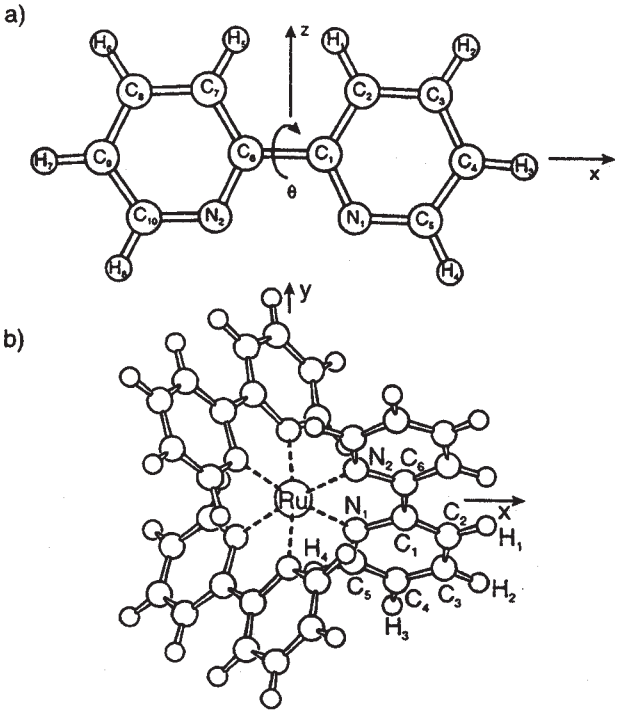

Figure 2. (a) *cis*-bpy and (b) $Ru(bpy)_3^{2+}$.

integrals involved have recently been described by J. J. P. Stewart.[8] In this article, we report the application of EDiT to a number of representative examples based on EHMO wave functions. We focus on the description of electronic charge-transfer transitions, which are actually of great interest and cannot be treated with the different popular ZDO (zero differential overlap) approaches. To warm up, we first consider formaldehyde and MnO_4^-.[3,9] We then discuss the oscillator strengths as a function of the torsional angle of *p*-(*N*,*N*-dimethylamino)benzonitrile (DMABN), which has become noted for its so-called twisted intramolecular charge-transfer (TICT) state.[10,11] An investigation of 2,2′-bipyridyl (bpy) as a function of the torsional angle serves as a starting point to discuss the $Ru(bpy)_3^{2+}$ spectrum. This will clarify some features

CHART 1: Structure of $[Co(CO)_4(H_7Si_8O_{12})]$

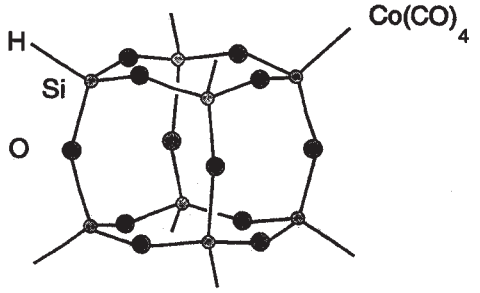

of the spectrum of this extensively studied complex. The first monosubstituted octasilasesquioxane with a silicon–metal bond has recently become available, namely, $[Co(CO)_4(H_7Si_8O_{12})]$.[12] It bears oxygen lone pair to cobalt charge-transfer transitions, which are discussed. The compounds under consideration are displayed in Figures 1 and 2 and in Chart 1.

2. Experimental Section

EDiT. The electronic transition–dipole moment ($\vec{\mu}_{nm}^{ed}$) between two wave functions ψ_n and ψ_m is defined as[1,13,14]

$$\vec{\mu}_{nm}^{ed} := \langle \psi_n | \vec{\mu}_{ed} | \psi_m \rangle \tag{1}$$

$$\vec{\mu}_{ed} = -(\sum_i e\vec{r}_i) \tag{2}$$

The oscillator strength (f) of the transition $n \leftarrow m$ amounts to

$$f = \frac{8\pi^2 \tilde{\nu} c m_e}{3he^2} |\vec{\mu}_{nm}^{ed}|^2 \tag{3}$$

Making use of the definition of the transition–dipole length (D_{nm})

$$|D_{nm}|^2 := \frac{1}{e^2} |\vec{\mu}_{nm}^{ed}|^2 \tag{4}$$

we find

$$f = l_0 \tilde{\nu} |D_{nm}|^2 \tag{5}$$

where e is the elementary charge, h is Planck's constant, m_e is the electron mass, c is the speed of the light in vacuum, $\vec{r}_i$ are the electron position vectors, $\tilde{\nu}$ is the wavenumber in cm^{-1} of the transition $n \leftarrow m$, and l_0 is equal to 1.085×10^{-5} cm/Å^2. f is dimensionless. The relation between the molar decadic extinction coefficient (ϵ) and the oscillator strength (f) can be expressed as follows:

$$f = 4.32 \times 10^{-9} \int_{band} \epsilon(\tilde{\nu})\, d\tilde{\nu} \tag{6}$$

where f is an intrinsic property of the species (molecule, compound, particle) under consideration and independent of the electromagnetic field responsible for the excitation. Typical f values for electronic dipole-allowed transitions, further denoted as f_{ed}, are in the range of 10^{-3}–1. The f_{ed} values for a single absorption or emission electron obey the sum rule[1]

$$\sum_i f_{ed}^{n_i \leftarrow m} = 1 \tag{7}$$

where i runs over all excited states involved. For the strongest electronic transitions, f_{ed} may therefore be in the order of 1. Generalizing this result leads to the rule that the summed up

oscillator strength in an electronic spectrum must be equal to the number of electrons in the molecule.

The LCAO−MO wave functions are written as products of one-electron molecular orbitals that may contain two electrons each with antiparallel spin. In can be shown that all electrons residing in closed shells do not affect the f_{ed} values.[13] Therefore, we can restrict the discussion to the two MOs changing their occupation upon excitation. We denote the initial and final MOs with ψ_i and ψ_f, respectively. f_{ed}^{fi} is proportional to the energy gap between the two MOs ψ_i and ψ_f, $\tilde{\nu}$, and to $|D_{fi}|^2$, but the factor l_0 has to be doubled if ψ_i is occupied by two electrons,[15] and hence, the maximum f_{ed} value possible for a transition between two nondegenerate molecular orbitals must be 2. Combining eqs 1 and 4, we find for the transition−dipole length

$$D_{fi} = \langle\psi_f|\vec{r}|\psi_i\rangle = \langle\sum_k c_k^f\chi_k|\vec{r}|\sum_s c_s^i\chi_s\rangle = \sum_{ks} c_k^f c_s^i\langle\chi_k|\vec{r}|\chi_s\rangle \quad (8)$$

where c_k^f and c_s^i are the coefficients of the atomic orbitals χ constituting the MOs. This equation can be written as a matrix containing integrals over atomic orbitals. We distinguish between block-diagonal or one-center and off-block-diagonal or two-center integrals. The block-diagonal elements contain AOs located at the same atom, while the off-block-diagonal elements concern AOs that are located at different centers. The calculation of the matrix elements is cumbersome. Our treatment basically relies on the procedure described in ref 13. However, for the sake of easier and generally valid programming, some effort was necessary to accommodate this method. The calculation of the transition−dipole length reduces to the computations of overlap integrals with modified Slater exponents, ζ. We use the overlap subroutine of ICON8[16] and ICONC&INPUTC[17] to calculate the overlap integrals to which the right transformation properties are applied. Slater-type overlap integrals have recently been investigated by Stewart.[8] Our computer program, which we name EDiT, has been restricted to FORTRAN 77 standards what makes it easily portable to most platforms.[18] EDiT reads input files created by ICONC&INPUTC.

We conclude this section by saying a few words about oscillator strengths of excitations between degenerate MOs. Any electron occupying the degenerate initial molecular orbital may be promoted to any molecular orbital of the degenerate final set. Hence, the formula for the f_{ed} value takes the following form:

$$f_{ed} = 2l_0\,\tilde{\nu}\,\frac{\bar{b}_i}{2}\cdot\frac{\sum_{n=1}^{G_f}\sum_{m=1}^{G_i}|\langle\psi_f^n|\vec{\mu}_{ed}|\psi_i^m\rangle|^2}{G_i} \quad (9)$$

where G_i and G_f indicate the degeneracy of the initial and the final MO, respectively. The averaged occupation number of the initial MO is denoted by $\bar{b}_i$; the 2 in the denominator takes into consideration that the factor $2l_0$ is again calculated for fully occupied orbitals. As it is only possible to promote one electron at a time which may originate from any of the initial molecular orbitals, we have to divide the double sum by G_i.

MO Calculations. Molecular orbital calculations have been carried out by the extended Hückel method.[4] The off-diagonal elements were calculated as[3a]

$$H_{ij} = {}^1/_2 kS_{ij}(H_{ii} + H_{jj}) \quad (10)$$

by using the weighted Wolfsberg−Helmholz formula[19] with a distance-dependent Hückel constant[20]

$$k = 1 + [\kappa + \Delta^2 - \Delta^4\kappa]e^{-\delta(R-d_0)} \qquad \Delta = \frac{H_{ii} - H_{jj}}{H_{ii} + H_{jj}} \quad (11)$$

H_{ii} and H_{jj} are the Coulomb integrals of the ith and the jth atomic orbital, respectively. R is the distance between the atoms where the ith and the jth atomic orbitals are located. d_0 is the sum of the ith and jth atomic orbital radii calculated from the corresponding Slater exponents; see eqs 13 and 14 in ref 20a. Standard $\kappa = 1$ and $\delta = 0.35$ Å^{-1} parameters were applied. To correct for the core−core repulsion, a two-body term as explained in ref 20a has been taken into account. The computations were carried out using the parameters in Table 1 and ref 12. For MnO_4^-, a population analysis based on ab initio calculations reveals that the population of the 3d orbitals is close to that of the Mn^{2+} ion in which two electrons have been removed from the 4s orbital. We have therefore applied the STO basis sets of the Mn^{2+} ion.[21] If not stated otherwise, the bond lengths and angles used for the calculations are compiled in Table 2. For the EHMO parameters and the geometry of $[Co(CO)_4(H_7Si_8O_{12})]$, we refer to ref 12.

Absorption Spectra. Absorption spectra were measured at room temperature on a PHILIPS PU 8740 scanning spectrophotometer. A 10-mm quartz cell was used. Bandwidth and scan speed were chosen to be 0.2 nm and 125 nm/min, respectively. The $[Ru(bpy)_3^{2+}](Cl^-)_2$ complex has been synthesized as described in ref 22, and its spectrum was measured in water. The ligand was purchased at Fluka and measured in acetonitrile, cyclohexane, ethanol (Merck p.a.), 2 M NaOH, and 0.1 M HCl.

TABLE 1: Coulomb Integrals H_{ii} and Slater Exponents ζ_i

element	AO	H_{ii}/eV	ζ_1	ζ_2	c_1	c_2
H	1s	−13.60	1.300			
C	2s	−21.40	1.710			
	2p	−11.40	1.625			
N	2s	−26.00	2.140			
	2p	−13.40	1.950			
Mn	4s	−10.03	1.650			
	4p	−6.06	1.150			
	3d	−12.43	5.150	2.100	0.547	0.605
Ru	5s	−9.23	2.080			
	5p	−5.78	2.040			
	4d	−12.14	5.380	2.300	0.534	0.637

TABLE 2: Bond Lengths and Angles[a]

compd	pt group	bond	length/Å	bond angle	angle/deg
H_2CO	C_{2v}	C−O	1.220	H_1−C−H_2	120.00
		C−H_1	1.080		
MnO_4^-	T_d	Mn−O_1	1.590	O_1−Mn−O_2	109.47
DMABN	C_{2v}	C_1−C_2	1.440	C_3−C_2−C_7	120.00
		C_{Ar}−C_{Ar}	1.395	C_5−N_2−C_8	120.00
		N_1−C_1	1.158	H_6−C_8−N_2	109.47
		C_5−N_2	1.426		
		N_2−C_8	1.472		
		C_{Ar}−H	1.084		
		C_8−H_6	1.093		
bpy	C_{2v}	C_{Ar}−C_{Ar}	1.392	C_{Ar}−C_{Ar}−C_{Ar}	120.00
		C_6−C_1	1.489	C_{Ar}−C_{Ar}−N	116.00
		C_{Ar}−N_{Ar}	1.338	H−C_{Ar}−C_{Ar}	120.00
		C_{Ar}−H	1.082		
$Ru(bpy)_3^{2+}$	D_3	Ru−N	2.048	C_{Ar}−C_{Ar}−C_{Ar}	120.00
		C_{Ar}−C_{Ar}	1.390	C_{Ar}−C_{Ar}−N	118.00
		C_{Ar}−N	1.335	H−C_{Ar}−C_{Ar}	120.00
		C_{Ar}−H	1.082		

[a] The data of refs 10e and 49 have been used for the planar structure of DMABN and for $Ru(bpy)_3^{2+}$, respectively.

TABLE 3: Matrix Elements of D_{fi} (in Å) for the $\pi^* \leftarrow \pi$ Transition of Formaldehyde Calculated for Three Different Origins of the Coordinate System

z	$0.5607(2p_{yC})$	$+0.7164(2p_{yO})$
$-0.8567\langle 2p_{yC}$	$+0.2930^a$	$+0.0120^a$
	$+0.0000^b$	$+0.0657^b$
	-0.5860^c	$+0.0417^c$
$+0.7315\langle 2p_{yO}$	-0.0180^a	$+0.3197^a$
	-0.0983^b	$+0.6393^b$
	-0.0624^c	$+0.0000^c$

[a] The origin at the middle of the C=O bond. [b and c] Origin at the carbon and at the oxygen atom, respectively.

3. Results and Discussion

Formaldehyde. We consider the z-polarized $\pi^* \leftarrow \pi$ transition of formaldehyde. The computed final and initial molecular orbitals (ψ_f and ψ_i) are

$$\psi_f = -0.8567(2p_{yC}) + 0.7315(2p_{yO})$$
$$\psi_i = 0.5607(2p_{yC}) + 0.7164(2p_{yO}) \qquad (12)$$

with an energy separation of approximately 42 500 cm^{-1}. The transition–dipole length (D_{fi}), eq 8, consists of four terms:

$$D_{fi,z} = \begin{pmatrix} -0.8567(0.5607)\langle 2p_{yC}|z|2p_{yC}\rangle & -0.8567(0.7164)\langle 2p_{yC}|z|2p_{yO}\rangle \\ 0.7315(0.5607)\langle 2p_{yO}|z|2p_{yC}\rangle & 0.7315(0.7164)\langle 2p_{yO}|z|2p_{yO}\rangle \end{pmatrix} \qquad (13)$$

The diagonal elements are of one-center nature, while the off-diagonal terms contain AOs located at different atoms and are therefore of the two-center type. We have calculated these elements for three different origins of the coordinate system: (a) origin in the middle of the C=O bond (Figure 1a); (b and c) origin at the carbon and at the oxygen atom, respectively. The results are reported in Table 3. We observe that the off-diagonal elements may become quite large, depending on the origin of the coordinate system. Because of the nature of the $\pi^* \leftarrow \pi$ transition, they are of different sign and almost cancel. They are, however, necessary to make the absolute value of the sum over all four matrix elements equal. The summation of the numerical values in Table 3 yields (a) |0.6067| Å, (b) |0.6067| Å, and (c) |−0.6067| Å. This means that the sum is independent of the chosen coordinate system, as required by theory. The oscillator strength of this transition amounts to

$$f_{ed,z} = (2l_0\ cm/Å^2)(42\ 500\ cm^{-1})(0.6067\ Å)^2 = 0.34 \qquad (14)$$

The reported experimental value of this $\pi^* \leftarrow \pi$ excitation is 0.3.[13] If we had chosen the ZDO approach, which neglects the off-block-diagonal elements, the three different $f_{ed,z}$ values (a) 0.35, (b) 0.38, and (c) 0.32 would have been obtained. This means that the full calculation is independent of the origin of the coordinates, as it should be, while the ZDO approach is not.

Permanganate Ion. The permanganate ion can be regarded as the classical charge-transfer coordination complex. Its electronic spectrum has been reported by many individuals and is still the focus of recent publications.[3,9,23,24] Three main absorption bands lie below 50 000 cm^{-1}, namely at 18 500, 32 200, and 44 000 cm^{-1}. We aim at the description of the oscillator strength of the long-wavelength band, responsible for the violet color. The highest occupied molecular orbital is of t_1 symmetry and thus 3-fold degenerate. The LUMO spans an E represenatation of the T_d point group, and thus, the first symmetry-allowed band is caused by a $e \leftarrow t_1$ transition between the oxygen t_1 orbitals and the e orbitals exhibiting mainly metal d character. Hence, this $^1T_2 \leftarrow {}^1A_1$ transition is of the LMCT type.[24] By group theoretical reasoning

$$E \otimes T_1 \supset T_2 \qquad \Gamma_{x,y,z} = T_2 \qquad (15)$$

the transition is equally allowed in any of the three directions $\vec{x}$, $\vec{y}$, and $\vec{z}$. The total transition–dipole moment ($\vec{\mu}^{ed}_{fi,r}$) must be independent of the chosen origin of the coordinate system, as we have already pointed out. This does not hold for its projections to the axes. Applying the proposition of Pythagoras, we get

$$\vec{\mu}^{ed}_{fi,r} = \sqrt{(\vec{\mu}^{ed}_{fi,x})^2 + (\vec{\mu}^{ed}_{fi,y})^2 + (\vec{\mu}^{ed}_{fi,z})^2} \qquad (16)$$

However, considering the choice of our coordinates as motivated by group theory[25]—the three axes coincide with the 2-fold symmetry axis (Figure 1b)—we expect $f_{ed,x} = f_{ed,y} = f_{ed,z}$. This is correct, as we see by inspection of the computations compiled in Table 4.

TABLE 4: Oscillator Strength of the First Electronic Transition (LUMO ← HOMO) of MnO_4^-

no.	no. of ψ_i	no. of ψ_f	$f_{ed,x}$	$f_{ed,y}$	$f_{ed,z}$
1	14	17	3.6687E-03	7.0006E-02	1.6455E-10
2	15	17	4.8758E-02	7.8430E-03	1.6455E-10
3	16	17	5.0485E-02	2.5065E-02	1.6455E-10
4	14	18	1.2233E-03	2.3338E-02	3.8998E-02
5	15	18	1.6257E-02	2.6136E-03	6.1764E-02
6	16	18	1.6833E-02	8.3600E-03	3.6489E-02
$\sum_{i=1}^{6}$			1.3723E-01	1.3723E-01	1.3725E-01
$\sum_{i=1}^{6}/G_i$			0.046	0.046	0.046

[a] $\Delta E_{cal} = 15\ 450\ cm^{-1}$.

TABLE 5: First Electronic Dipole-Allowed Transition ($^1T_2 \leftarrow {}^1A_1$) of MnO_4^-

	expt[3a]	ref 3a	ab initio[21]	EDiT
ΔE/eV	2.29	1.68	2.48	1.92
$f_{ed,x} = f_{ed,y} = f_{ed,z}$	0.032	0.076	0.069	0.046

Our calculation yields a HOMO/LUMO separation of 15 450 cm^{-1} or 1.92 eV, which is too small and could be adjusted. We have not done this since it is natural for the orbital energy difference which does not contain the exchange intergral to be smaller than the energy difference between the ground state and the excited state.[26] The experimental f_{ed} values projected to the axes (i.e., $f_{ed,x}$, $f_{ed,y}$, $f_{ed,z}$) of the first electronic transition in permanganate lie at 0.032.[3a] Our calculated f_{ed} value is 0.046 by taking the full transition matrix into account. The ZDO approach, which considers only the one-center elements, yields 0.057. This means that the off-block-diagonal elements correct the ZDO f_{ed} value significantly.

The initial MO is 3-fold-degenerate and the final MO is 2-fold-degenerate, respectively, giving rise to six transitions. These values are summed up and divided by three; see eq 9. The experimental absorption energy of the LUMO ← HOMO transition in MnO_4^- is 18 470 cm^{-1}.

To our knowledge, we are the first to calculate the oscillator strength of the long-wave transition ($^1T_2 \leftarrow {}^1A_1$) in MnO_4^-, applying an exact treatment within the extended Hückel method. Wolfsberg and Helmholz neglected the oxygen 2s AOs to reduce the computational burden and obtained a wrong ordering of the t_2 and e levels in the LUMO region.[24] They computed a projected oscillator strength of 0.076 considering only the block-diagonal elements. An f_{ed} value of 0.069 was obtained in a

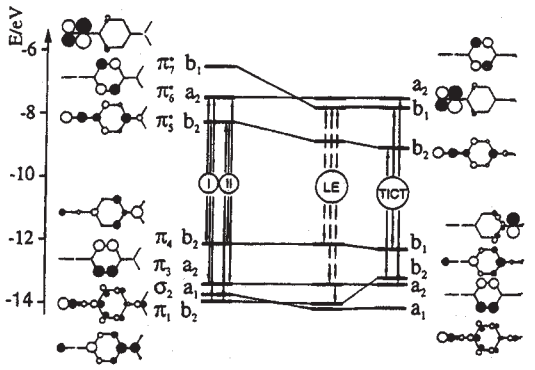

Figure 3. Correlation diagram (frontier orbital region) for DMABN. The values for the amino group torsional angle and the C≡N bond length are as follows: (left) 0°, 1.16 Å; (center) 0°, 1.26 Å; (right) 90°, 1.26 Å.

more recent ab initio study in which ψ_{A_1} and ψ_{T_2} were built from occupied and virtual orbitals of a ground-state calculation.[21] These results are compiled in Table 5.

DMABN. The phenomenon of the dual fluorescence of *p*-(*N*,*N*-dimethylamino)benzonitrile (DMABN) and structurally related compounds in polar solvents has given rise to scientific controversy over its origin which has been going on for the last 4 decades.[10,11] While Majumdar et al. were to stress the relevance of full ground-state geometry optimization in their study on DMABN,[10e] Calzaferri et al.[11] pointed out that the relaxation of the $S_1 \leftarrow S_0$ Franck–Condon (FC) excitation leads to a lengthening of the C≡N bond by an amount of about 0.1 Å, allowing the cyano-group-centered π^* orbital to contribute significantly to the developing locally excited (LE) state which has been reported to be important for the description of the evolving TICT state. This is the starting point for an EDiT oscillator strength calculation of the $\pi^*_{(A)} \leftarrow \pi_{(D)}$ charge-transfer transition between intramolecular π-acceptor/π-donor groups.

To explain the calculations, we first consider the frontier orbitals depicted in Figure 3. On the left-hand side, we start from the planar S_0 ground state of DMABN with the first two sets of $\pi^* \leftarrow \pi$ transitions. Set I represents the *x*-polarized $\pi^*(a_2) \leftarrow \pi(b_2)$ and $\pi^*(b_2) \leftarrow \pi(a_2)$ excitations, giving rise to the S_1 state of B_1 symmetry. Set II represents the *z*-polarized $\pi^*(b_2) \leftarrow \pi(b_2)$ and $\pi^*(a_2) \leftarrow \pi(a_2)$ excitations, giving rise to the S_2 state of A_1 symmetry.[10c] CI treatment to create the desired transitions between electronic states, namely, the *x*-allowed $S_1(B_1) \leftarrow S_0(A_1)$ and the *z*-allowed $S_2(A_1) \leftarrow S_0(A_1)$ transitions, would not be a difficult problem mathematically,[13] but there is no way to circumvent appropriate parameterization. We therefore prefer to discuss the results on a one-electron basis, which leads to an interesting pictorial interpretation. We present the results within the C_{2v} point group; thus, the *z* axis coincides with the 2-fold rotational axis C_2, and *x* lies in the plane of the aromatic ring. This allows a simplified discussion without losing important information.

In the ground-state geometry on the left side of Figure 3, $\pi^*(b_1)$ is too high in energy to be directly attainable in a FC excitation. However, occupation of the C≡N antibonding π^* orbital causes weakening of this bond. As the FC geometry relaxes by stretching the C≡N bond, the energy of the b_1 symmetry in-plane orbital π^* decreases rapidly, by as much as 1.2 eV during stretching of 0.1 Å. Thus, π^* becomes the superjacent LUMO. As a result, its contribution to the developing partial CT state increases rapidly and the molecule ends up in the LE state displayed in Figure 3, with broken arrows indicating electronic-dipole-forbidden relaxation pathways.

Starting from the LE state, we now consider torsion of the dialkylamino group 90° out-of-plane. The main event observed is that the $\pi_4(b_2)$ orbital changes in character to become an in-plane, amino-group-centered orbital of b_1 symmetry. The destabilization of the π_1 orbital should also be noted. It influences the character of the highest occupied molecular orbital in the HOMO region. With increasing weight of the A_1 symmetry $(b_1)^1(b_1)^1$ configuration in the new state, which is assigned to the TICT state, the charge separation becomes more complete. Stabilization of this state is enhanced by solvent polarity.[10]

TABLE 6: Results of the Oscillator Strength Calculation of DMABN[a]

	TICT($f_{ed,z}$)		$\pi^* \leftarrow \pi$ ($f_{ed,z}$)	
torsion angle	$(b_1) \leftarrow (b_1)$	$(b_1) \leftarrow (b_2)$	$(b_2) \leftarrow (b_2)$	$(a_2) \leftarrow (a_2)$
90°	4.468E-03	2.381E-36	9.464E-01	5.318E-01
75°	4.324E-03	1.160E-01	8.423E-01	5.320E-01
60°	3.988E-03	3.597E-01	6.299E-01	5.316E-01
45°	3.738E-03	5.210E-01	4.935E-01	5.320E-01
30°	2.553E-03	7.648E-01	2.988E-01	5.319E-01
15°	8.850E-04	8.689E-01	2.202E-01	5.330E-01
0°	2.393E-38	9.040E-01	2.006E-01	5.324E-01

[a] The symmetry labels refer to MO symmetries in the ideal TICT geometry (torsion angle 90°).

The weight of the low-energy excited configurations of A_1 symmetry increases from left to right in Figure 3, due to the large stabilization of the π^* orbital, the destabilization of the π_1 orbital, and the change in character of the π_4 orbital from b_2 to b_1. A *z*-polarized $(b_1) \leftarrow (b_1)$ transition is symmetry-allowed. Calculating the oscillator strengths shows, however, that it is low in intensity. This is evident from the data in Table 6 where we report EDiT oscillator strengths for the four relevant transitions $(b_1) \leftarrow (b_1)$, $(b_2) \leftarrow (b_1)$, $(b_2) \leftarrow (b_2)$, and $(a_2) \leftarrow (a_2)$ at different values of the amino group torsional angle. The low intensity of the *z*-allowed transition $(b_1) \leftarrow (b_1)$ is not surprising and can be explained by the poor overlap of the π^* and π_4 orbitals. The intrinsic emissive lifetime (τ_0) for the f → i emission is

$$1/\tau_0 = \frac{64\pi^4\tilde{\nu}^3}{3h}|\langle\psi_i|e\vec{r}|\psi_f\rangle|^2 \qquad (17)$$

where $\tilde{\nu}$ is the wavenumber in cm^{-1} of the luminescence f → i and $\vec{r}$ is the electron position vector.[13] Substituting eq 3 in eq 17 leads to

$$1/\tau_0 = \frac{8\pi^2\tilde{\nu}^2e^2}{cm_e}f_{ed} \qquad (18)$$

Hence, the TICT state is expected to live long enough to relax to a state described by the $(b_1)^1(b_2)^1$ configuration. Emission of a photon in this state is forbidden by symmetry; see Table 6. However, a small twist of only 15° increases this oscillator strength along the *z* axis enormously. TICT emission has empirically been shown to be *z*-polarized and strong in intensity, and the emission rates can be activated thermally.[10] This is in good qualitative agreement with the oscillator strength calculations. We note that the two *z*-polarized $\pi^* \leftarrow \pi$ transitions depend relatively little on the amino group torsional angle. This dependence is indeed characteristic for the TICT state.

2,2′-Bipyridyl. Pauling estimated the C_1-C_6 double-bond order in diphenyl as 10%.[27] The distance between the two bridging atoms in bpy (Figure 2a) is approximately 0.01 Å longer, thus implying an even smaller double-bond character. Hence, rotation of the two rings should be easy. X-ray studies reveal that the trans conformation is realized in the crystalline state.[28] However, formation of the cis conformation happens

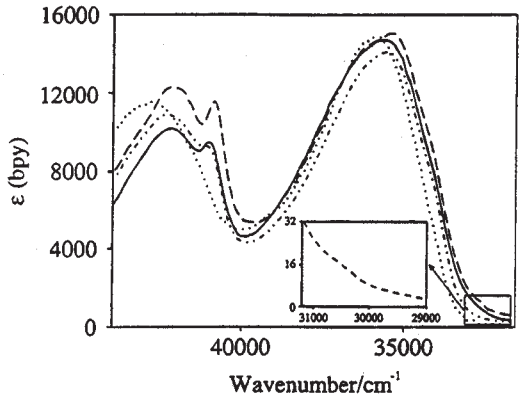

Figure 4. Absorption spectra of bpy in cyclohexane (dashed), acetonitrile (solid), ethanol (dash-dot), and 2 M NaOH (dotted) at room temperature. The ϵ values are in L·mol^{-1}·cm^{-1}.

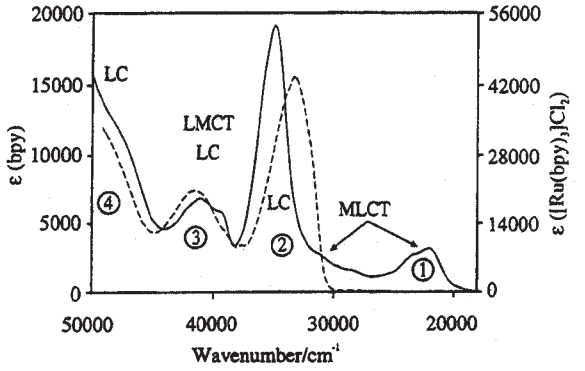

Figure 5. UV/vis absorption spectra of $Ru(bpy)_3^{2+}$ in H_2O (solid) and bpy in 0.1 M HCl (dashed). The ϵ values are in L·mol^{-1}·cm^{-1}.

without a large activation barrier upon coordination to a metal center. We calculated $\Delta E^{\ddagger} = 0.24$ eV for the trans-to-cis conversion. This is only half of, e.g., the boat-to-chair interconversion barrier of cyclohexane. Fielding and Le Fèvre have carried out dipole moment measurements of bpy in benzene from which they conclude that its geometry is near-trans with a ring−plane twist of about 28° or $\theta = 152°$.[29] $\theta = 0$ refers to the cis-planar geometry. Our EHMO calculations give no evidence for a local minimum in the range of $90° \leq \theta < 180°$. We observe a local minimum at $\theta = 14°$ and the global minimum at $\theta = 180°$, in qualitative agreement with recently published ab initio studies on the torsional potential of the 4,4′-bipyrimidine.[30] It is therefore most likely that Fielding's experimental results have to be interpreted as caused by a mixture of trans and cis isomers. Because of the shallow potential along the angle θ, it appears probable that intermediate angles are populated to a certain degree depending on the solvent and on the temperature. This conclusion is supported by results from UV/vis spectroscopy.

Nakamoto was the first to report the pH dependence of the electronic absorption spectrum of bpy.[31] In acidic solution, two bands are observed, one at 33 200 cm^{-1} and another one at 41 500 cm^{-1}. Krumholz,[32] and later also Westheimer and Benfey,[33] showed that the monocation predominates in 2 N HCl. In basic solution, the authors reported two peaks at 35 850 and 43 100 cm^{-1}, respectively, which they assigned to the trans isomer. It was argued that the monocation favors a not completely planar cis geometry, while in basic solution the planar trans isomer is the most stable form. Some further aspects of the UV/vis spectrum of bpy have been discussed based on PPP calculations by Gondo[34] and by Hanazaki and Nagakura.[35]

In Figure 4, we show the ultraviolet absorption spectra of bpy in acetonitrile, cyclohexane, ethanol, and 2 M NaOH and in Figure 5 the spectrum of $Ru(bpy)_3^{2+}$ in water along with the bpy spectrum in 0.1 M HCl. We notice that the first band of bpy appears at the same position and is of similar shape in cyclohexane, acetonitrile, ethanol, and 2 M NaOH and that it is very broad and featureless in each case. Three main bands at about 35 500, 41 100, and 42 200 cm^{-1} are observed in organic solvents and only two at 35 500 and 42 600 cm^{-1} in 2 M NaOH. The main absorptions in 0.1 M HCl appears at 33 200 and 41 500 cm^{-1}, and we also note the much less intense band at 37 500 cm^{-1}, Figure 5.

The results of EDiT calculations on bpy as a function of the angle θ are compiled in Table 7 and in Figure 6. In Figure 7, we show the correlation diagram of the frontier MOs of *trans*- and *cis*-bpy. The two prominent $\pi^* \leftarrow \pi$ absorptions of the cis isomer can be assigned to the $1\pi^* \leftarrow 1\pi$ and the $2\pi^* \leftarrow 1\pi$ transitions with calculated oscillator strengths of 0.853 and 0.376. The $2\pi^* \leftarrow 2n$ transition is very weak ($f_{ed} = 10^{-5}$) for cis, but becomes the prominent $1\pi^* \leftarrow 1\pi$ band for trans. We follow the $1\pi^* \leftarrow 1\pi$ transition, circles in Figure 6, along the angle θ starting at $\theta = 0°$. The orbital energy difference between the $1\pi^*$ and 1π levels increases with increasing θ. At the same time, the oscillator strength decreases rapidly at angles larger than about 30°. If we surpass $\theta = 90°$, it correlates with the $2\pi^* \leftarrow 2\pi$ transition of the trans isomer and its energy leaves the spectral region considered here. Instead a new $1\pi^* \leftarrow 1\pi$ transition develops out of the former $2\pi^* \leftarrow 2n$ which gains much intensity at $\theta > 90°$ and almost reaches the $1\pi^* \leftarrow 1\pi$ oscillator strength of the cis-planar conformation, while the orbital energy difference decreases to approximately the same value. The reverse is true for the cis $2\pi^* \leftarrow 1\pi$ (squares in Figure 6) which retains its $\pi^* \leftarrow \pi$ character but loses intensity with increasing θ and becomes symmetry-forbidden at $\theta = 180°$. The second excited π^* state of the trans isomer has to be regarded as a mixture of the $(b_g 1\pi)^1(a_u 3\pi^*)^1$ and the $(b_g 3\pi)^1$-$(a_u 1\pi^*)^1$ configurations which have the same symmetry, similar oscillator strength, and similar energy and can therefore interact. They correlate, however, only with high-energy configurations at decreasing θ and are therefore not indicated in Figure 6 but are reported in Table 7.

If we accept the results of our calculations and conclusions of previous studies that trans is the stable isomer but that the potential along the angle θ is very shallow, then it is easy to understand why the first intense band in Figure 4 is broad, featureless, and similar in all four solvents. It is caused by a superposition of bands arising from an equilibrium Boltzmann distribution over the whole range of angles θ from 180° to 0°. This causes a hypsochromic shift of the maximum of the first intense band, because the $1\pi^* \leftarrow 1\pi$ transition energies of the species with angles different from $\theta \approx 180°$ to $\theta \approx 0°$ appear at larger energy; see Figure 6. The reason for the bathochromic shift of the first $1\pi^* \leftarrow 1\pi$ transition by 2300 cm^{-1} of the protonated bpy is due to the predominance of the cis isomer and hence a narrow Boltzmann distribution of the θ region close to 0°.

We now investigate if this explanation is consistent with the other observations. Let us remark that the calculated orbital energy differences are always smaller than the experimental electronic transition energies, for the same reason as explained for MnO_4^-, but it is generally observed that the energy differences between the first and the second transitions are well reproduced as long as CI plays a minor role.[7a,b]

The second intense band of bpy appears at about the same position, ≈42 200 cm^{-1}, and is of similar shape in cyclohexane, acetonitrile, ethanol, and 2 M NaOH. It is broad, featureless,

TABLE 7: Transition Energies and Oscillator Strengths of the First $\pi^* \leftarrow \pi$ and $\pi^* \leftarrow$ n Transitions of *cis*- and *trans*-bpy[a]

cis-bpy (C_{2v})					*trans*-bpy (C_{2h})				
trans	sym	pol	ΔE_{cal}	f_{ed}	trans	sym	pol	ΔE_{cal}	f_{ed}
				$\pi^* \leftarrow \pi$					
$1\pi^* \leftarrow 1\pi$	B_1	x	30 361	0.853	$1\pi^* \leftarrow 1\pi$	B_u	x	30 511	0.848
$1\pi^* \leftarrow 2\pi$	A_1	z	37 318	0.018	$1\pi^* \leftarrow 1\pi$	B_u	z	30 511	0.013
$2\pi^* \leftarrow 1\pi$	A_1	z	38 100	0.376	$1\pi^* \leftarrow 3\pi$	B_u	z	39 723	0.453
					$3\pi^* \leftarrow 1\pi$	B_u	z	41 085	0.502
				$\pi^* \leftarrow$ n					
$1\pi^* \leftarrow 1$n	B_2	y	27 850	3.2×10^{-4}	$1\pi^* \leftarrow 1$n	A_u	y	27 078	2.6×10^{-4}
$2\pi^* \leftarrow 2$n	B_2	y	37 326	1.0×10^{-5}	$3\pi^* \leftarrow 1$n	A_u	y	37 651	8.7×10^{-5}
$3\pi^* \leftarrow 1$n	B_2	y	37 890	1.3×10^{-4}	$2\pi^* \leftarrow 2$n	A_u	y	37 838	1.1×10^{-5}

[a] ΔE_{cal} is given in cm^{-1}. The axes of the coordinate systems are chosen as depicted in Figure 2a.

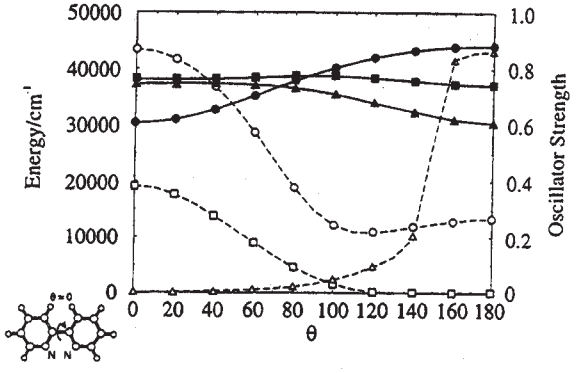

Figure 6. Orbital energies (solid lines) and oscillator strengths (dashed lines) of the main electronic transitions of bpy as a function of θ. θ = 0° (cis): $1\pi^* \leftarrow 1\pi$ (circles), $2\pi^* \leftarrow 1\pi$ (squares), and $2\pi^* \leftarrow$ 2n (triangles). θ = 180° (trans): $1\pi^* \leftarrow 1\pi$ (triangles), $1\pi^* \leftarrow 2\pi$ (squares), and $2\pi^* \leftarrow 2\pi$ (circles).

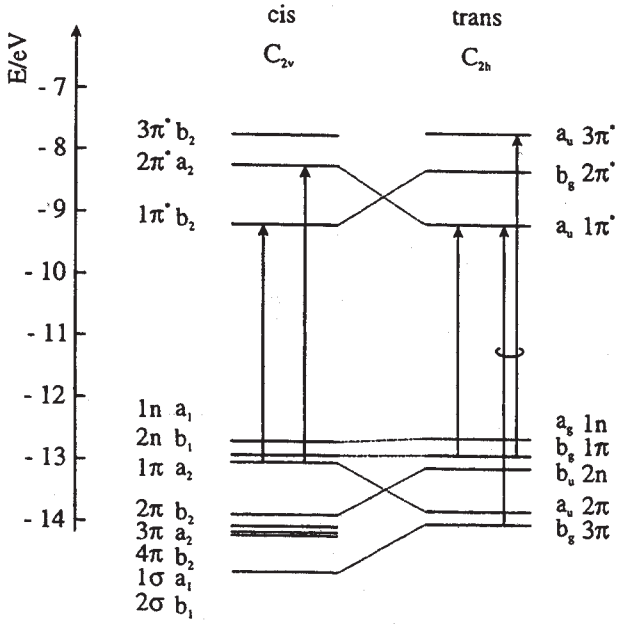

Figure 7. Frontier orbital correlation diagram of *cis*- and *trans*-bpy.

and of about half the intensity of the first $\pi^* \leftarrow \pi$ transition. In addition, there is a weaker bathochromically shifted band at 41 100 cm^{-1} the intensity of which decreases in the order cyclohexane > acetonitrile > ethanol > 2 M NaOH and becomes the prominent band in 0.1 M HCl. Based on our calculations, both bands have to be interpreted as the second $\pi^* \leftarrow \pi$ transition, the higher energetic one belonging to the trans and the lower energetic to the cis isomer. This means that the ratio of the intensities of these bands is an indicator for the ratio of the cis conformation, preferred by the protonated

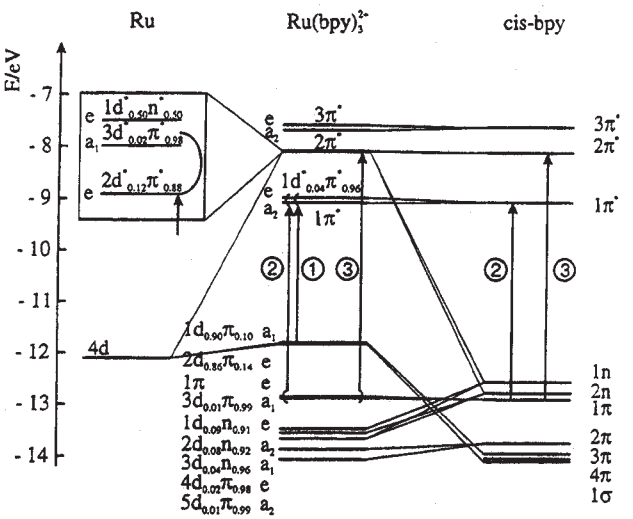

Figure 8. Comparison of the one-electron levels of the *cis*-bpy (C_{2v}) and the 4d levels of Ru with those of $Ru(bpy)_3^{2+}$ (D_3) based on a FMO analysis. The subscripts x and y ($x + y = 1$) in the $d_x\pi_y$ and d_xn_y labels are the populations per electron. The e(d*) is energetically very close to the a_1 and e levels emerging from the $2\pi^*$ orbital of bpy. These three levels are therefore enlarged in the box to the left. Main electronic transitions are indicated by arrows.

bpy, and the trans isomer. Different bpy−solvent interactions affect the Boltzmann population of the angle θ. One can speculate that detailed experimental investigations of the bpy spectra in different solvents and in a sufficiently large temperature range would allow us to determine this Boltzmann distribution experimentally. At present, we can only deduce that the concentration of the cis form decreases in the order 0.1 M HCl > cyclohexane > acetonitrile > ethanol > 2 M NaOH. The small peak at 37 500 cm^{-1} observed in 0.1 M HCl can probably be assigned to the $1\pi^* \leftarrow 2\pi$ transition of the cis isomer with a calculated oscillator strength of 0.018, see Table 7, but this remains uncertain.

The first electronically-excited-state configuration of bpy is of the $(1n)^1(1\pi^*)^1$ type. According to the results reported in Table 7, a $\pi^* \leftarrow$ n transition should appear as a long-wavelength shoulder of the $1\pi^* \leftarrow 1\pi$ band. However, it is well-known that the energy of the $\pi^* \leftarrow$ n transitions strongly depends on the solvent polarity, which has been investigated for the comparable terpyridyl (tpy) molecule by Fink and Ohnesorge.[36] They have observed the solvent dependence of the long-wavelength tail of the tpy absorption spectrum as typically expected for $\pi^* \leftarrow$ n transitions. The tpy $\pi^* \leftarrow$ n absorption starts at 420 nm in cyclohexane and nearly disappears below the $\pi^* \leftarrow \pi$ band in chloroform. We have therefore investigated the long-wavelength tail of bpy below 32 000 cm^{-1}. The onset in Figure 4 shows a shoulder at 31 500 cm^{-1} in cyclohexane, which we could not observe in the other solvents. It is therefore

TABLE 8: Calculated Transition Energies (in cm^{-1}) and Oscillator Strengths for the $Ru(bpy)_3^{2+}$ Complex[a]

type	ΔE_{cal}	transition	sym	f_{ed}	total
MLCT	22 312	$1\pi^* \leftarrow 2d_{0.86}\pi_{0.14}$	E	0.06	0.13 (1)
	23 070	$1d_{0.04}^{\delta}\pi_{0.96}^{\delta} \leftarrow 2d_{0.86}\pi_{0.14}$	E	0.07	
	29 905	$2d_{0.12}^{\delta}\pi_{0.88}^{\delta} \leftarrow 1d_{0.90}\pi_{0.10}$	E	0.07	
	30 152	$2d_{0.12}^{\delta}\pi_{0.88}^{\delta} \leftarrow 2d_{0.86}\pi_{0.14}$	A_2	0.09	0.16 (1 + 2)
	30 287	$3d_{0.02}^{\delta}\pi_{0.98}^{\delta} \leftarrow 2d_{0.86}\pi_{0.14}$	E	0.06	
	33 307	$2\pi^* \leftarrow 1d_{0.90}\pi_{0.10}$	A_2	0.07	
	34 025	$3\pi^* \leftarrow 1d_{0.90}\pi_{0.10}$	E	0.03	0.08 (2)
	34 272	$3\pi^* \leftarrow 2d_{0.86}\pi_{0.14}$	A_2	0.01	
MC	30 130	$1d_{0.50}^{\delta}n_{0.50}^{\delta} \leftarrow 1d_{0.90}\pi_{0.10}$	E	0.01	0.02 (2)
	30 377	$1d_{0.50}^{\delta}n_{0.50}^{\delta} \leftarrow 2d_{0.86}\pi_{0.14}$	A_2	0.02	
LC	31 000	$1\pi^* \leftarrow 1\pi$	E	0.08	
	31 137	$1\pi^* \leftarrow 3d_{0.01}\pi_{0.99}$	A_2	0.54	
	31 759	$1d_{0.04}^{\delta}\pi_{0.96}^{\delta} \leftarrow 1\pi$	A_2	0.52	1.13 (2)
	31 759	$1d_{0.04}^{\delta}\pi_{0.96}^{\delta} \leftarrow 1\pi$	E	0.10	
	31 896	$1d_{0.04}^{\delta}\pi_{0.96}^{\delta} \leftarrow 3d_{0.01}\pi_{0.99}$	E	0.21	
	36 282	$1d_{0.04}^{\delta}\pi_{0.96}^{\delta} \leftarrow 2d_{0.08}n_{0.92}$	E	0.04	
	38 841	$2d_{0.12}^{\delta}\pi_{0.88}^{\delta} \leftarrow 1\pi$	E	0.10	0.44 (3)
	38 975	$3d_{0.02}^{\delta}\pi_{0.98}^{\delta} \leftarrow 1\pi$	E	0.12	
	38 978	$2d_{0.12}^{\delta}\pi_{0.88}^{\delta} \leftarrow 3d_{0.01}\pi_{0.99}$	E	0.18	
	43 036	$2d_{0.12}^{\delta}\pi_{0.88}^{\delta} \leftarrow 1d_{0.09}n_{0.91}$	A_2	0.05	
	43 036	$2d_{0.12}^{\delta}\pi_{0.88}^{\delta} \leftarrow 1d_{0.09}n_{0.91}$	E	0.01	0.10 (4)
	43 364	$2d_{0.12}^{\delta}\pi_{0.88}^{\delta} \leftarrow 2d_{0.08}n_{0.92}$	E	0.04	
	43 498	$3d_{0.02}^{\delta}\pi_{0.98}^{\delta} \leftarrow 2d_{0.08}n_{0.92}$	A_2	0.04	
LMCT	39 066	$1d_{0.50}^{\delta}n_{0.50}^{\delta} \leftarrow 1\pi$	E	0.04	0.07 (3)
	39 202	$1d_{0.50}^{\delta}n_{0.50}^{\delta} \leftarrow 3d_{0.01}\pi_{0.99}$	E	0.03	
	43 261	$1d_{0.50}^{\delta}n_{0.50}^{\delta} \leftarrow 1d_{0.09}n_{0.91}$	E	0.17	
	43 261	$1d_{0.50}^{\delta}n_{0.50}^{\delta} \leftarrow 1d_{0.09}n_{0.91}$	A_2	0.07	0.68 (4)
	43 588	$1d_{0.50}^{\delta}n_{0.50}^{\delta} \leftarrow 2d_{0.08}n_{0.92}$	E	0.51	

[a] The numbers in parentheses refer to the labels in Figure 5.

likely that this shoulder can be assigned to the $1\pi^* \leftarrow 1n$ transition of the trans isomer with an oscillator strength in the order of 3×10^{-4}.

Tris(2,2′-bipyridyl)ruthenium(II). The excited-state chemistry of $Ru(bpy)_3^{2+}$ has attracted intense interest in recent years, and as a consequence, its electronic spectrum has been investigated in great detail.[22,37-46] It is therefore difficult to add relevant new information. However, EHMO–EDiT calculations offer new insight which helps to improve our understanding of this interesting complex, the one-electron levels of which are depicted in Figure 8. The comparison of the $Ru(bpy)_3^{2+}$ frontier orbitals with those of the ligand and the metal has been obtained by means of the fragment molecular orbital (FMO) technique.[47] The subscripts x and y ($x + y = 1$) in the $d_x\pi_y$ and d_xn_y labels are the populations of these orbitals per electron as derived from a Mulliken population analysis.[48] The Ru 4d orbitals mix strongly with the n-type ligand orbitals to form the metal-to-ligand bond and at the same time to push the e(d*) levels above the first four π^* ligand orbitals which are only slightly perturbed. We name the e(d*) wave function d–n* orbital based on the $d_{0.5}n_{0.5}$ population. Each ligand π^* orbital is split into a degenerate e set and a MO of either a_1 or a_2 symmetry upon coordination to the metal center. The nondegenerate component of these orbitals can be classified to be either symmetric a_1 or antisymmetric a_2 with respect to the C_2 axis retained in the complex. Weak interaction of the Ru t_{2g}-(d) orbitals with the 3π and 1σ MOs of bpy split them by 250 cm^{-1} into an a_1(d) and an e(d) component, namely, $a_1(1d_{0.90}\pi_{0.10})$ and $e(2d_{0.86}\pi_{0.14})$, upon symmetry reduction from O_h to D_3. The experimental value for the a_1(d)-to-e(d) splitting is 200 cm^{-1}.[40]

The electronic spectrum of $Ru(bpy)_3^{2+}$ can be grouped into four regions phenomenologically by visual inspection of the spectrum in Figure 5 and also based on the MO diagram in

TABLE 9: First Electronic MLCT Transitions in $Ru(bpy)_3^{2+}$ [a]

∥MLCT			⊥MLCT		
trans	ΔE_{cal}	f_{ed}	trans	ΔE_{cal}	f_{ed}
$a_2 \leftarrow a_1$	22 065	6.49×10^{-3}	$a_2 \leftarrow e$	22 312	6.48×10^{-2}
			$e \leftarrow a_1$	22 823	1.36×10^{-3}
$e \leftarrow e$	23 070	1.60×10^{-3}	$e \leftarrow e$	23 070	7.41×10^{-2}

[a] The ratio $I_\perp/I_\parallel$ is calculated to be 17.3. ΔE_{cal} in cm^{-1}.

CHART 2: Overlap Population between the Nitrogen Atoms of the Three bpy's at the Geometry of $Ru(bpy)_3^{2+}$

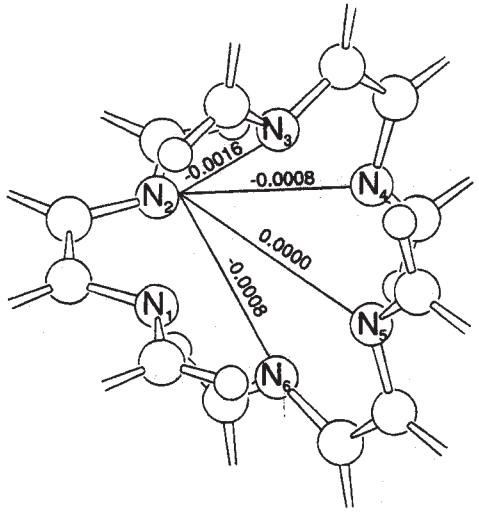

Figure 8. However, the number of possible excited-state configurations in the HOMO/LUMO region give rise to $13 \times 11 = 143$ different one-electron transitions in any of the three directions. Even though a few of them are forbidden by symmetry, most are allowed, but many are of low intensity. Transitions with oscillator strengths larger than 1.0×10^{-2} and energies smaller than 45 000 cm^{-1} are compiled in Table 8. We have grouped them according to the usual classifications MLCT($\pi^* \leftarrow$ d), MC(d* $\leftarrow$ d), LC($\pi^* \leftarrow \pi$, $\pi^* \leftarrow$ n), and LMCT(d* $\leftarrow \pi$, d* $\leftarrow$ n). It is obvious that a very detailed analysis in which spin–orbit and CI interactions would have to be included is complicated. Being aware of the danger of oversimplification, we nevertheless deduce a general pattern.

The first two electronic transitions are of the $\pi^* \leftarrow$ d type with similar oscillator strength. They are polarized perpendicular with respect to the C_3 axis and lead to the so often investigated MLCT($\pi^* \leftarrow$ d) states. Taking a closer look at the MLCT transitions in the HOMO/LUMO region, see Table 9, we find that the first band is strongly polarized perpendicular to the C_3 axis, which is not surprising as this is in the direction metal to ligand.[39] The calculated intensity ratio $I_\perp/I_\parallel$ of this long-wavelength part of the MLCT transition is 17.3. Palmer and Piper measured polarized spectra of single crystals and reported a ratio of 26.5 at 300 K.[22] The good agreement between the calculated energy range of 22 065 to 23 070 cm^{-1} and the accepted experimental value of 22 120 cm^{-1} of this first MLCT transition should not be overemphasized but gives us some confidence that the parameters in Table 1 are reasonable.

This long-wavelength part of the MLCT region is followed by three transitions located in the gap between the regions 1 and 2 in Figure 5. They are all of the MLCT($\pi^* \leftarrow$ d) type. Their total oscillator strength is 0.16 (Pythagoras) and hence overcomes the total f_{ed} value of the first MLCT region. They are mainly responsible for the long tail or shoulders at 31 055 and 29 070 cm^{-1} and not the much weaker MC transitions which play a minor role.

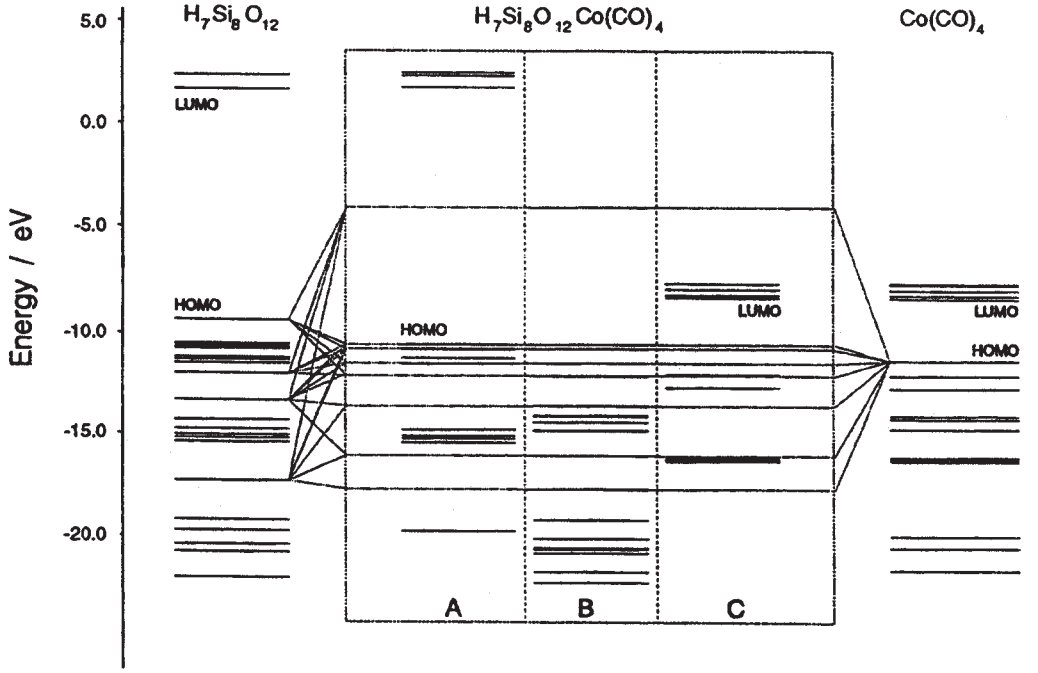

Figure 9. Correlation diagram for $H_7Si_8O_{12} + Co(CO)_4 \rightarrow [(H_7Si_8O_{12})Co(CO)_4]$. The energy levels of $[(H_7Si_8O_{12})Co(CO)_4]$ are split into three parts. Parts A and C contain the orbitals localized on the $H_7Si_8O_{12}$ and on the $Co(CO)_4$ fragment, respectively. The MOs of region B are delocalized over the whole molecule.

The third MLCT($\pi^* \leftarrow$ d) bands are buried by the intense LC transitions and are therefore expected to affect the dipolar character of the spectral region 2. This is in good agreement with recently measured Stark absorption spectra of the bpy ligand and the corresponding Zn^{2+}, Fe^{2+}, Ru^{2+}, and Os^{2+} complexes.[46] Hug and Boxer have found that the intraligand transitions of the complexes lead to excited states with much larger dipole moments than expected for purely ligand-centered transitions.

The LC region spans from 31 000 cm^{-1} to the far-UV. The most intense part is centered around 31 137 cm^{-1} and indicated with the label 2 in Figure 5 and Table 8. It is expected to be of similar shape and energy as the $1\pi^* \leftarrow 1\pi$ transition of *cis*-bpy. The bathochromic shift can be explained by the weak but not negligible interaction of the metal orbitals with the $1\pi^*$ and 1π orbitals of the ligand. The direct through-space interaction between the three bpy ligands is very weak as indicated by the reduced overlap population between the N atoms; see Chart 2. We should not ignore, however, that this first LC($\pi^* \leftarrow \pi$) band consists of five significant contributions, while there is only one $1\pi^* \leftarrow 1\pi$ transition in the cis-planar ligand.

The next intense part of the LC region groups around 38 975 cm^{-1}. It is indicated with the label 3 in Figure 5 and Table 8. At about the same energy, we observe two relatively intense LMCT (d$-$n$^* \leftarrow 1\pi$; d$-$n$^* \leftarrow 3d\pi$)-type transitions. The spectrum in Figure 5 shows two bands in this region. Because of the small energy difference, it is difficult to know if these transitions have to be attributed to the shoulder at 39 400 cm^{-1}, but it seems probable if we take the relative oscillator strength into account. In any case, however, we feel that the often encountered opinion that this region has to be attributed to a MLCT transition should be revised. We add that the calculated ratio of the oscillator strength of regions 2 and 3 is 2.56 for the complex and 2.27 for the ligand. This and the comparison with the spectrum of the bpy monocation in Figure 5 support our interpretation. Region 4 in Figure 5 lies very high for a frontier orbital description. However, a LMCT(d$-$n$^* \leftarrow$ n)-type transition seems to contribute significantly to this absorption. This means that its similarity with the ligand spectrum should not be overemphasized. The two intense LMCT transitions are calculated to lie at 43 261 and 43 588 cm^{-1} with oscillator strengths of 0.17 and 0.51, respectively. The transferred charge is of σ origin and the large intensity is due to the extended overlap between the donor and acceptor MOs.

Monosubstituted Octanuclear Silasesquioxane. The electronic structure of this complex which has recently been synthesized[12] can be best understood by splitting it into three parts as shown in Figure 9. The orbitals localized on the $H_7Si_8O_{12}$ and on the $Co(CO)_4$ fragments are denoted by A and C; those delocalized over the whole molecule are denoted as B. The main correlations between the fragments and the delocalized molecular orbitals of region B are indicated with dotted lines. The orbitals of region B are responsible for the bonding and antibonding interactions between $H_7Si_8O_{12}$ and $Co(CO)_4$; see ref 12. Experimentally, the UV/vis spectrum of $[Co(CO)_4(H_7Si_8O_{12})]$ measured in *n*-hexane at room temperature starts with a long tail at about 380 nm which develops after some weak shoulders to a first maximum below 200 nm. Since the HOMO region consists of oxygen lone-pair orbitals, we can attribute the first transitions to be of the charge-transfer type in which an electron of the HOMO region A is transferred to the LUMO region of C:

$$[H_7Si_8O_{12}][Co(CO)_4] \xrightarrow{h\nu} [H_7Si_8O_{12}]^+[Co(CO)_4]^- \qquad (19)$$

Individual oscillator strengths for the long-wavelength tail A-to-C charge-transfer transitions have been calculated to be at best 1.5×10^{-3}. The two highest occupied orbitals of region B belong mainly to the $H_7Si_8O_{12}$ fragment and are about 90% oxygen lone pair character with some Co contribution. This means that the shorter wavelength B-to-C transitions are of the same $H_7Si_8O_{12}$ (oxygen lone pair) to $Co(CO)_4$ fragment charge-transfer type. The individual oscillator strengths of these B-to-C charge-transfer transitions, however, have been calculated to be up to 0.03.

Acknowledgment. We acknowledge financial support by the Schweizerische Nationalfonds zur Förderung der wissenschaftlichen Forschung grant No. 20-34042.92 and by the Swiss Federal Office of Energy BEW grant No. (93)034. The calculations were performed on an IBM RS/6000 workstation provided by IBM Corporation on terms of a Joint Study Agreement.

References and Notes

(1) Mulliken, R. S. *J. Chem. Phys.* **1939**, *7*, 20.

(2) (a) Pariser, R.; Parr, R. G. *J. Phys. Chem.* **1953**, *21*, 466 and 767. (b) Pople, J. A. *Trans. Faraday Soc.* **1953**, *49*, 1375. (c) Fabian, J.; Mehlhorn, A.; Zahradník, R. *Theoret. Chim. Acta* **1968**, *12*, 247.

(3) (a) Wolfsberg, M.; Helmholz, L. *J. Chem. Phys.* **1952**, *20*, 837. (b) Ballhausen, C. J.; Gray, H. B. *Molecular Orbital Theory*; W. A. Benjamin: Amsterdam, 1965. (c) Holt, S. L.; Ballhausen, C. J. *Theoret. Chim. Acta* **1967**, *7*, 313.

(4) Hoffmann, R. *J. Chem. Phys.* **1963**, *39*, 1397.

(5) (a) Hoffmann, R.; Woodward, R. B. *Acc. Chem. Res.* **1968**, *1*, 17. (b) Hoffmann, R. *Acc. Chem. Res.* **1971**, *4*, 1. (c) Hoffmann, R. *A Chemist's View of Bonding in Extended Structures*; Verlag Chemie: Weinheim, 1988. (d) Calzaferri, G.; Hoffmann, R. *J. Chem. Soc., Dalton Trans.* **1991**, 917. (e) Wong, Y.-T.; Schubert, B.; Hoffmann, R. *J. Am. Chem. Soc.* **1992**, *114*, 2367.

(6) (a) Zinola, C. F.; Ariva, A. J.; Estiu, G. L.; Castro, E. A. *J. Phys. Chem.* **1994**, *98*, 7566. (b) Nikolov, G. S. *Inorg. Chem.* **1994**, *33*, 1144. (c) Magonov, S. N.; Whangbo, M.-H. *Adv. Mater.* **1994**, *6*, 355. (d) Gorinchoi, N. N.; Bersuker, I. B.; Polinger, V. Z. *New. J. Chem.* **1993**, *17*, 125. (e) Albright, T. A.; Burdett, J. K.; Whangbo, M. H. *Orbital Interactions in Chemistry*; John Wiley & Sons: New York, 1985. (f) Siddarth, P.; Marcus, R. A. *J. Phys. Chem.* **1990**, *94*, 2985. (g) Gleiter, R. *J. Chem. Soc. A* **1970**, 3174. (h) Gleiter, R. *Angew. Chem.* **1974**, *86*, 770.

(7) (a) Calzaferri, G.; Grüninger, H.-R. *Helv. Chim. Acta* **1979**, *62*, 1112. (b) Amouyal, E.; Mouallem-Bahout, M.; Calzaferri, G. *J. Phys. Chem.* **1991**, *95*, 7641. (c) Brändle, M.; Calzaferri, G. *Res. Chem. Intermed.* **1994**, *20*, 783. (d) Bärtsch, M.; Calzaferri, G.; Marcolli, C. *Res. Chem. Intermed.* **1995**, *6*, 577. (e) Calzaferri, G.; Marcolli, C. *J. Phys. Chem.* **1995**, *99*, 3895.

(8) Stewart, J. J. P. *J. Comp.-Aided. Mol. Design* **1990**, *4*, 1.

(9) Sradnov, V. I.; Harrison, W. T. A.; Gier, T. E.; Stucky, G. D.; Popitsch, A.; Gatterer, K.; Markgraber, D.; Fritzer, H. P. *J. Phys. Chem.* **1994**, *98*, 4673.

(10) (a) Grabowsky, Z. R.; Rotkiewicz, K.; Siemiarczuk, A.; Cowley, D. J.; Baumann, W. *Nouv. J. Chim.* **1979**, *3*, 443. (b) Lippert, E.; Rettig, W.; Bonacic-Koutecky, V.; Heisel, F.; Miehé, J. A. *Adv. Chem. Phys.* **1987**, *68*, 1. (c) Lafemina, J. P.; Duke, C. B.; Paton, A. *J. Chem. Phys.* **1987**, *87*, 2151. (d) Van der Auweraer, M.; Grabowski, Z. R.; Rettig, W. *J. Phys. Chem.* **1991**, *95*, 2083. (e) Majumdar, D.; Sen, R.; Bhattacharyya, K.; Bhattacharyya, S. P. *J. Phys. Chem.* **1991**, *95*, 4324. (f) Rettig, W.; Majenz, W.; Lapouyade, R.; Haucke, G. *J. Photochem. Photobiol. A: Chem.* **1992**, *62*, 415. (g) Weersink, R. A.; Wallace, S. C. *J. Phys. Chem.* **1994**, *98*, 10710.

(11) Bergamasco, S.; Calzaferri, G.; Hädener, K. *J. Photochem. Photobiol. A: Chem.* **1992**, *66*, 327.

(12) Calzaferri, G.; Imhof, R.; Törnroos, K. W. *J. Chem. Soc., Dalton Trans.* **1993**, 3741.

(13) McGlynn, S. P.; Vanquickenborne, L. G.; Kinoshita, M.; Carroll, D. G. *Introduction to Applied Quantum Chemistry*; Holt, Rinehart and Winston: New York, 1972.

(14) Herzberg, G. *Molecular Spectra and Molecular Structure. I Spectra of Diatomic Molecules*; Van Nostrand Reinhold: New York, 1950.

(15) Kuhn, H. *J. Chem. Phys.* **1958**, *29*, 958.

(16) Howell, J.; Rossi, A.; Wallace, D.; Haraki, K.; Hoffmann, R. *ICON8, Quantum Chemistry Program Performing extended-Hückel Calculation*; Quantum Chemical Program Exchange, QCPE No. 344, 1978.

(17) Calzaferri, G.; Brändle, M. *ICONC&INPUTC*; Quantum Chemical Program Exchange, QCPE No. 116 1992, update May 1993.

(18) A copy of the program is available on request.

(19) Ammeter, J. H.; Bürgi, H.-B.; Thibeault, J. C.; Hoffmann, R. *J. Am. Chem. Soc.* **1978**, *100*, 3686.

(20) (a) Calzaferri, G.; Forss, L.; Kamber, I. *J. Phys. Chem.* **1989**, *93*, 5366. (b) Brändle, M.; Calzaferri, G. *Helv. Chim. Acta* **1993**, *76*, 924.

(21) Ziegler, T.; Rauk, A.; Baerends, E. J. *J. Chem. Phys.* **1976**, *16*, 209.

(22) Palmer, R. A.; Piper, T. S. *Inorg. Chem.* **1966**, *5*, 864.

(23) (a) Carrington, A.; Symons, M. C. *Chem. Rev.* **1963**, *63*, 443. (b) Jørgensen, C. K. *Absorption Spectra and Chemical Bonding in Complexes*; Addison-Wesley: Reading, MA, 1962. (c) Teltow, J. Z. *Phys. Chem.* **1938**, *B40*, 397. (d) Teltow, J. Z. *Phys. Chem.* **1939**, *B43*, 198.

(24) Viste, A.; Gray, H. B. *Inorg. Chem.* **1964**, *3*, 1113.

(25) Cotton, F. A. *Chemical Applications of Group Theory*, 3rd ed.; John Wiley & Sons: New York, 1993.

(26) Calzaferri, G. In *Photochemical and Photoelectrochemical Conversion and Storage of Solar Energy*; Tian, Z. W., Cao, Y., Eds.; International Academic: Beijing, 1992; p 141.

(27) Pauling, L. *Nature of the Chemical Bond*; Cornell University: Ithaca, NY, 1945.

(28) Cagle, F. W. *Acta Crystallogr.* **1948**, *1*, 158.

(29) Fielding, P. E.; Le Fèvre, R. J. *J. Chem. Soc.* **1951**, 1811.

(30) Barone, V.; Cauletti, C.; Piancastelli, M. N.; Ghedini, M.; Toscano, M. *J. Phys. Chem.* **1991**, *95*, 7217.

(31) Nakamoto, K. *J. Phys. Chem.* **1960**, *64*, 1420.

(32) Krumholz, P. *J. Am. Chem. Soc.* **1951**, *73*, 3487.

(33) Westheimer, F. H.; Benfey, O. T. *J. Am. Chem. Soc.* **1956**, *78*, 5309.

(34) Gondo, Y. *J. Chem. Phys.* **1964**, *41*, 3928.

(35) Hanazaki, I.; Nagakura, S. *Inorg. Chem.* **1968**, *8*, 648.

(36) Fink, D. W.; Ohnesorge, W. E. *J. Phys. Chem.* **1970**, *74*, 72.

(37) (a) Sauvage, J.-P.; Collin, J.-P.; Chambron, J.-C.; Guillerez, S.; Coudret, C.; Balzani, V.; Barigelletti, F.; De Cola, L.; Flamigni, L. *Chem. Rev.* **1994**, *94*, 993. (b) Balzani, V.; Bolletta, F.; Gandolfi, M. T.; Maestri, M. *Top. Curr. Chem.* **1978**, *75*, 1. (c) Juris, A.; Balzani, V.; Barigelletti, F.; Campagna, S.; Belser, P.; von Zelewsky, A. *Coord. Chem. Rev.* **1988**, *84*, 85. (d) Schönherr, T.; Degen, J.; Gallhuber, E.; Hensler, G.; Yersin, H. *Chem. Phys. Lett.* **1989**, *158*, 519.

(38) Kalyanasundaram, K. *Coord. Chem. Rev.* **1982**, *46*, 159.

(39) Felix, F.; Ferguson, J.; Güdel, H. U.; Ludi, A. *Chem. Phys. Lett.* **1979**, *62*, 153.

(40) Lytle, F. E.; Hercules, D. M. *J. Am. Chem. Soc.* **1969**, *91.I*, 253.

(41) Crosby, G. A.; Hipps, K. W.; Elfring, W. H., Jr. *J. Am. Chem. Soc.* **1974**, *96*, 629.

(42) Carroll, P. J.; Brus, L. E. *J. Am. Chem. Soc.* **1987**, *109*, 7613.

(43) (a) Myrick, M. L.; Blakley, M. K.; DeArmond, M. K.; Arthur, M. L. *J. Am. Chem. Soc.* **1988**, *110*, 1325. (b) DeArmond, M. K.; Myrick, L. M. *Acc. Chem. Res.* **1989**, *22*, 364.

(44) Kober, E. M.; Meyer, T. J. *Inorg. Chem.* **1984**, *23*, 3877.

(45) Oh, D. H.; Boxer, S. G. *J. Am. Chem. Soc.* **1989**, *111*, 1130.

(46) Hug, S. J.; Boxer, S. G. In preparation.

(47) Imamura, A. *Mol. Phys.* **1969**, *15*, 225.

(48) Mulliken, R. S. *J. Chem. Phys.* **1955**, *23*, 1833.

(49) Rillema, D. P.; Jones, D. S.; Levy, H. A. *J. Chem. Soc., Chem. Commun.* **1979**, 849.

JP9501557